Struct Multidisc Optim (2009) 38:627–641
DOI 10.1007/s00158-008-0303-y

INDUSTRIAL APPLICATION

Optimal electrode shaping for precise modal electromechanical filtering

A. Elka · I. Bucher

Received: 18 March 2008 / Revised: 1 July 2008 / Accepted: 19 July 2008 / Published online: 22 August 2008

Abstract This paper addresses the optimal shape design of segmented spatial sensors and actuators that isolate selected mode shapes and perform modal filtering. Electromechanical filters have reappeared with the new manufacturing capabilities of micro-electro-mechanical structures (MEMS). In such small dimensions it proves essential to treat their elastic behaviour as continuous rather than discrete systems that require suitable design methods, some of which are developed here. In MEMS filters, the input signal is converted to external electrostatic forces and in order to perform the desired filtering, the electrodes need to be shaped such that they excite only a desired part of the dynamics. An optimization scheme that shapes these electrodes to achieve optimal filtering is developed. In order to enhance the filter's performance and minimize energy lost to the supporting structure, a special support tuning method is proposed. Several simulated examples examine the effectiveness of the proposed optimization methods.

Keywords Optimization · Modal filter · Quarter wavelength · MEMS filter · Electrode shaping

A. Elka · I. Bucher (✉)
Mechanical Engineering, Technion, Israel institute of Technology, Haifa 32000, Israel
e-mail: bucher@technion.ac.il

A. Elka
e-mail: elka@technion.ac.il

1 Introduction and literature survey

An extended modal filter concept essentially similar to the one described in Gawronski (1998) is adopted for structural vibration synthesis of a MEMS filter application. A modal filter uses spatial shaping of the excitation to selectively affect only certain modes while other modes of vibrations are not excited. Modal sensors/actuators electrodes are proposed and developed to be incorporated into flexible vibrating structures. The electrodes act as a transducer to convert mechanical vibrations into electrical signal and vice versa, a comprehensive summary can be found in Tilmans (1996). The layout and shape of the distributed sensors and actuators electrodes can be easily computed in theory, but, in practice, inevitable constraints such as the need to realize the electrodes in segments render the theoretical solution far from ideal. This paper addresses the optimal shape design of distributed sensors and actuators electrodes. It is shown that a precise model-based optimization stage, overcomes the problems that the implementation of the theoretical solution creates. The proposed approach can help in a trimming stage that is based on real measurements where the electrode's gap is perturbed until local optimum is achieved.

This work provides an optimization method that overcomes the limitations of truncated and segmented modal electrodes. Applications like filters in (radio frequency) RF MEMS make use of modal decomposition to better control or modify the vibratory behaviour of a multi-degree of freedom (MDOF) MEMS structures. Unfortunately, the truncated (segmented) modal actuators/sensors pose some difficulties to control only

a selected mode in a desired frequency range. The orthogonality condition is not fulfilled when part of the excitation vector are forced to zero which is what happens when the actuator or sensor are made of segments. In addition, the electrostatic force can only create attractive forces thus one is compelled to split the electrodes. We suggest a new optimization based design method for reshaping of the spatially distributed electrodes.

When the structural parameters change, for example, due to manufacturing tolerances or drift in the boundary conditions, the model is no longer accurate and the spatial electrodes become imperfect. With the proposed approach the spatial electrodes can be trimmed to adjust the performance of the filter until sufficiently good performance is restored. It is thus suggested to create a calibrated error correction mechanism that can be realized with, say, a comb-drive with suspensions, John et al. (2003). Most previous works, making use of truncated left-eigenvectors, did not address the inaccuracy caused by the truncation hence did not suggest a general solution for it. A partial solution to the truncation problem of these electrodes was proposed in Friswell (1999) The proposed method is demonstrated in several examples. In the first example a numerical simulation of a one dimensional beam is provided; the second example consists of a 3D MEMS structure.

MEMS structures can have complicated geometry and only numerical modelling e.g. finite-elements (FE) can adequately capture its dynamics. In practice there are some discrepancies between the analytical model and the real structure, the numerically obtained modal vectors are an approximation therefore in situ trimming is essential. Contamination due to unmodelled dynamics can lead to the excitation of spurious vibration modes as can be seen in Nguyen et al. (2000). These spurious modes arise due to imprecise modelling and their effect can be reduced by means of optimized reshaping of the forcing electrodes, as shown here.

Most transducers measure simultaneously the entire response which is a combination of modes. When one wishes to extract the contribution of an individual mode, often a discrete array of sensors has to be employed with some spatial filtering. The use of a discrete array has several shortcomings: firstly it complicates the hardware since each sensor requires its own electronics and secondly the discrete nature of the array can result in spatial aliasing. The numerical signal processing of such an array, limits the frequency-range of this device, considerably.

On the other hand, spatial filtering which is performed by a continuous modal actuator or a modal sensor, generates the required filtered output with no additional processing and is therefore fast and inexpensive. Modal transducers, or modal sensors and modal actuators are described in the work of Preumont (1997) and Friswell (2001) or modal filter in Zhang et al. (1990). The latter describes the useful orthogonality of the modal filters. The benefit in using the left-eigenvectors is that we can eliminate unwanted modes and control the dynamics of the system, see Bucher and Braun (1993). The basic idea behind this concept is that a force whose distribution is proportional to the left eigenvectors, act as a modal force and it selectively controls the matching mode Zhang et al. (1990), Bucher and Braun (1993, 1997). This approach is known (although different terminology is being used) in control applications as modal control and it can be generalized to control a set of modes simultaneously as shown in Gawronski (1998).

Several publications refer to modal excitation methods and a representative summary can be found in Michael and Mauro (2001). Detailed information on the concept of shaped sensors is available in Preumont (1997) and Preumont et al. (2003). An alternative approach based on the concepts of controllability and observability to design modal transducers is defined in Gawronski (1998, 2000). Transducers obtained by the methods mentioned above are required to cover the whole extent of the structure and act on all the structural degrees of freedom (DOF), which is something not feasible.

Segmented transducers were investigated by Friswell (1999), the optimization of the sensor shape is carried out by minimizing an objective function of the curvature of the sensor's shape with constraints that enforces modal orthogonality to a desired mode. Michael and Mauro (2001) claims that this method is not always applicable and the orthogonality constraint is difficult to satisfy.

Zhuang and Baras (1994) have used the minimization of the stored energy in the system as a cost function to determine the optimal sensor shape for smart structure control. A genetic algorithm was used by Kim and Ryou (2002), Kim et al. (2000) in the optimization of the PVDF electrode by optimizing the gain distribution.

Callahan and Baruh (1996, 1999) applied active control with modal sensors from segmented piezoelectric simple shape elements with intelligent configuration on plates and circular cylindrical shells.

Modal filtering using an equally segmented piezoelectric film sensor and a weight was determined to minimize a cost function have been applied by Takagi et al. (2001) are not generally applicable for real time vibration control and has a problem of spatial aliasing.

Experiments with modal sensors with an array of PVDF segments were also done by Mao (2004).

This work seeks to reshape the forcing electrodes by optimizing the total response. This approach enhances the orthogonality of the eigenvectors were applicable but attacks the problem of inaccuracy on a more fundamental level.

The structure of the paper is as following: first a brief introduction to the relevant theory is provided. In Sections 3 & 4 we present examples for solving the optimization problem by model simulations that implement the theory and finally we show the effect of optimization on cancellation of poles with zeros.

2 Theoretical background-modelling of the problem

This chapter briefly considers left and right eigenvectors of linear vibrating systems. The formulation of distributed forces and sensors makes use of these quantities. Passive vibrating mechanical systems can be described by

$$\mathbf{M}\ddot{\mathbf{q}}(t) + \mathbf{D}\dot{\mathbf{q}}(t) + \mathbf{K}\mathbf{q}(t) = \mathbf{B}\mathbf{u}(t), \mathbf{q}(t) \in \mathbb{R}^n \tag{1}$$

Where: $\mathbf{q}$ contains the generalized degrees of freedom, $\mathbf{M}$, $\mathbf{K}$, $\mathbf{D}$ are the mass, stiffness and damping matrices respectively. The input matrix $\mathbf{B} \in \mathbb{R}^{n\times m}$ represents the spatial distribution for the external force $\mathbf{u}(t)$. Similarly, we can define physical outputs $\mathbf{y}(t)$ by an observation equation

$$\mathbf{y}(t) = \mathbf{C}\mathbf{q}(t) \tag{2}$$

which relates the internal degrees of freedom (DOFs) $\mathbf{q}$ to the actually measured quantities (outputs) by the output matrix $\mathbf{C} \in \mathbb{R}^{m\times n}$.

The frequency response function (FRF), relates the input and output in the frequency domain by a summation of the individual modes, Gawronski (1998).

$$\mathbf{H}(\omega) = \sum_{j=1}^{n} \frac{\mathbf{C}\boldsymbol{\phi}_j\boldsymbol{\phi}_j^T\mathbf{B}}{\omega_j^2 + 2i\zeta_j\omega_j\omega - \omega^2} \tag{3}$$

The computation of the transfer matrix $\mathbf{H}(\omega)$ using modal analysis is greatly facilitated by the use of modal coordinates $\boldsymbol{\eta}$ and modes $\boldsymbol{\Phi}$, defined by $\mathbf{q} = \boldsymbol{\Phi}\boldsymbol{\eta}$, Gawronski (1998).

The transfer function can be decomposed to two modal contributions, first as the modal output $\mathbf{C}\phi_j$ and second the modal input $\phi_j^T\mathbf{B}$. It is important to understand that we can control the shape of the transfer function by the level of each contribution and by the damping.

This paper uses the most common approach of viscous damping where the instantaneous generalized velocities are the only relevant state variables that affect damping forces. It has been shown, e.g. Geradin and Rixen (1998), He and Fu (2001), that light damping resulting in small coupling between the modes. In fact light damping can be either hysteretic or viscous and still produce nearly identical results. In the particular application, the designers strive to keep the damping levels as low as possible by evacuating the air and using materials with low internal losses. For this reason, the proportional damping model seems to be adequate.

2.1 Left mode shapes vs. right mode shapes—definitions

This section treats the undamped structure where $\mathbf{D} = 0$ in (1). The displacement related right mode shapes ϕ_r come from the solution of the eigenvalue problem:

$$\mathbf{M}^{-1}\mathbf{K}\phi_r = \omega_r^2\phi_r \qquad r = 1\ldots n \tag{4}$$

The left-eigenvectors $\boldsymbol{l}_r^T$ describe the modal force's spatial distribution that excites the response proportional to a specific right mode shape, Bucher and Braun (1993, 1997).

The left mode shapes are computed from:

$$\boldsymbol{l}_r^T\mathbf{M}^{-1}\mathbf{K} = \omega_r^2\boldsymbol{l}_r^T \qquad r = 1\ldots n \tag{5}$$

Defining $\mathbf{L} \triangleq \mathbf{M}\boldsymbol{\Phi}$

One obtains from the bi-orthogonality relations of modes, Strang (2006).

$$\boldsymbol{\Phi}^T = \mathbf{L}^{-1},\ \mathbf{L}^T = \boldsymbol{\Phi}^{-1} \tag{6}$$

The orthonormality property can be expressed as:

$$\boldsymbol{l}_r^T\boldsymbol{\phi}_r = \delta_{j,r} = \begin{cases} 1 & j = r \\ 0 & j \neq r \end{cases} \tag{7}$$

In particular, a specific mode is affected by selecting the force vector to be parallel to the matching left-eigenvectors, i.e., The general form of the modal force is $\mathbf{f}(\mathbf{t}) = \alpha(t)\,\boldsymbol{l}_j$ where: $j \in \{1\ldots n\}$, thus only the response due to ϕ_j is influenced by the force and $\alpha(t) \triangleq V\sin(\omega t)$ is a scalar representing the sinusoidal amplitude applied to the modal actuator.

2.2 Using a modal actuator and a modal sensor to excite and sense a single mode

We can select the modes to be excited by determining the actuation force's $\mathbf{f}(\mathbf{t})$ spatial distribution. Rewriting

(1) in the modal equation form using the transformation $\mathbf{q}(t) = \mathbf{\Phi}\boldsymbol{\eta}$, $\mathbf{\Phi} \in \mathbb{R}^{n\times n}$, $\eta \in \mathbb{R}^n$:

$$\ddot{\eta}_r + \omega_r^2 \eta_r = \phi_r^T \mathbf{f}(\mathbf{t}) \quad r \in \{1 \ldots n\} \tag{8}$$

Define $\alpha(t)$ as a scalar representing the sinusoidal amplitude applied to the modal actuator:

$$\alpha(t) \triangleq V \sin(\omega t) \tag{9}$$

Thus, the modal actuator force:

$$\mathbf{f}(\mathbf{t}) = V \sin(\omega t)\, \mathbf{M}\phi_r \tag{10}$$

This force distribution affects only the rth mode and is therefore a modal filter.

The modal sensor which isolates mode p can be constructed by selecting $r = p$ in such a way that

$$c = \boldsymbol{\phi}_p^T \mathbf{M} = \boldsymbol{l}_p^T \tag{11}$$

Thus, in this case

$$c\mathbf{q}(t) = \eta_p(t) \tag{12}$$

Therefore mode number p is extracted and filtered by the modal sensor.

2.3 The electrostatic force—spatial distribution and the electrode gap

In the previous section it was shown that forces proportional to the left vectors can isolate particular modes. It will be shown here how to use this information to design the geometry of an electrode that actuates and senses a specific mode shape.

The electrostatic force's spatial distribution has to be computed for a desired mode ϕ_n as shown below:

The electrostatic force for the parallel plate actuator, neglecting the fringe field, Bao (2000) is:

$$f_e = \frac{\varepsilon \mathrm{A}\,(V_{\mathrm{dc}} + V_{\mathrm{ac}} \sin(\omega \mathrm{t}))^2}{2\,(d_0 + y)^2} \tag{13}$$

where: ε is the permeability coefficient, V_{dc} the DC bias voltage, V_{ac} the AC voltage amplitude, A the electrode area and $d_0 + y$ is the gap when the structure undergoes a deformation y.

Performing a Taylor expansion for the small parameter y ($y \ll d_0$), and keeping the first term, (13) can be approximated by:

$$f_e \approx -\frac{1}{4d_0^2}\varepsilon A\Big(-2V_{\mathrm{dc}}^2 - 4V_{\mathrm{dc}}V_{\mathrm{ac}}\sin(\omega \mathrm{t}) - V_{\mathrm{ac}}^2 + V_{\mathrm{ac}}^2 \cos(2\omega \mathrm{t})\Big) \tag{14}$$

Defining:

$$V_{\mathrm{con}} = \varepsilon A V_{\mathrm{dc}} V_{\mathrm{ac}} \tag{15}$$

One can separate the geometry from the applied voltage levels

$$f_e = \frac{V_{\mathrm{con}}}{d_0^2} \tag{16}$$

The desired force distribution is described by a vector of generalised loads that correspond to the generalised DOF on each element. These forces can be interpolated using the element shape functions to produce a continuous distribution. From this distribution, the geometry of the electrode gap can be derived from (16)

$$d_{\mathbf{0}} = \sqrt{\left|\frac{V_{\mathrm{con}}}{f_{\mathbf{e}}}\right|} \tag{17}$$

The gap between the structure and the electrode is thus computed according to (17).

2.4 Electrode optimization algorithm

Unfortunately, RF-MEMS structures use segmented spatial modal sensors/actuators electrodes thus only a truncated spatial force that is an approximation of a left eigenvector can be applied and the modal filter becomes inexact. A method to overcome the inherent limitations of a practical implementation by optimally trimming the actuators and sensors electrode shape is developed here. The optimization process assists in obtaining the desired mode shapes of the structure while attenuating others by means of the proposed sub-optimal modal filtering.

The ideal full modal electrodes and the truncated modal electrodes produce a frequency response. Defining: $\mathbf{H_f}$—the transfer function of ideal full modal electrodes system, and $\mathbf{H_t}$—the transfer function of truncated modal electrodes system. It is clear that truncation will result in the excitations of undesired modes.

It is our goal to trim the truncated electrode such that the FRF becomes as close as possible to the ideal one. Thus we have to find the minimum of

$$J = \min \int_{-\infty}^{\infty} |\mathbf{H_f} - \mathbf{H_t}|^2 d\omega \tag{18}$$

Thus minimizing the mean-square of the difference in the response. Naturally a frequency range and weighting function can be employed to (18), see Skelton (1988) for more details.

2.4.1 Lyapunov equation approach for structural response optimization

During the optimization process the cost function in (18), it needs to be evaluated many times. Practical vibrating structures are represented by thousands of degrees of freedom in order to form valid models. To make the optimization process practical, the optimization scheme must compute the cost function and its derivatives efficiently in a reasonable amount of time.

In this section, a Lyapunov equation based approach is applied to the analysis of input–output characteristics for linear time invariant systems under the excitation of wide band (white noise) input, as shown in Skelton (1988).

Every time one wishes to compute the cost function (18), the Lyapunov equation has to be solved. Although this equation has a high order, it can still be solved efficiently, as described in the following section. The results can be readily applied to the evaluation of RMS responses in the optimization scheme.

In general, we have to minimize the response by minimizing its spectrum

$$\min \int_{-\infty}^{\infty} \left|\mathbf{y}(f)\right|^2 df \tag{19}$$

The performance criterion is an integral on the vibration amplitude response. Under random excitation, we define the mean-square (MS) value cost function

$$J = E\left[\mathbf{y}(t)\,\mathbf{y}^{\mathbf{T}}(t)\right] \tag{20}$$

The state covariance matrix satisfies the Lyapunov algebraic equation (Skelton 1988):

$$\mathbf{AX} + \mathbf{XA}^{\mathbf{T}} + \mathbf{Q} = 0 \tag{21}$$

$\mathbf{X}$, the solution for (21) is in fact the covariance matrix of the state. Having solved (21) we can evaluate the cost function via: $J = \mathbf{CXC}^T$.

2.4.2 Evaluating the performance criterion efficiently during the optimization

In order to evaluate the cost function J from (18), both the full and the truncated models are represented by a state-space model.

The optimal shapes of the continuously distributed sensor and actuator electrode gaps are determined through minimizing the residual vibration energy of the difference between an ideal full system and a truncated system over the admissible correction shape function space with no constraints. An algorithm has been developed to determine the optimal sensor and actuator electrode layout.

In order to evaluate the performance criterion we use the Lyapunov (21), where:

$$\mathbf{A} = \begin{bmatrix} \mathbf{0} & \mathbf{I} \\ -\mathbf{M}^{-1}\mathbf{K} & -\mathbf{M}^{-1}\mathbf{D} \end{bmatrix}, \mathbf{B} = \begin{bmatrix} \mathbf{0} \\ \mathbf{M}^{-1} \end{bmatrix}, \mathbf{Q} = \mathbf{B}W\mathbf{B}^{\mathbf{T}} \tag{22}$$

We use an input $u(t)$ which is a white noise process that has the variance:

$$W = cov\,(u) \triangleq \sigma^2 = 1 \tag{23}$$

When the dynamical system is expressed in a state-space form, it yields, for the full system having a full DOFs vector, the following equation:

$$\begin{aligned} \dot{\mathbf{x}}_1 &= \mathbf{Ax}_1 + \mathbf{B}_1\mathbf{u} \\ \mathbf{y}_1 &= \mathbf{C}_f\mathbf{x}_1 \end{aligned} \tag{24}$$

and for the truncated system having a truncated DOFs vector, the following equation:

$$\begin{aligned} \dot{\mathbf{x}}_2 &= \mathbf{Ax}_2 + \mathbf{B}_2\mathbf{u} \\ \mathbf{y}_2 &= \mathbf{C}_t\mathbf{x}_2 \end{aligned} \tag{25}$$

Augmenting (24) and (25) the difference in response can be written as

$$\begin{Bmatrix} \dot{\mathbf{x}}_1 \\ \dot{\mathbf{x}}_2 \end{Bmatrix} = \begin{bmatrix} \mathbf{A} & \mathbf{0} \\ \mathbf{0} & \mathbf{A} \end{bmatrix} \begin{Bmatrix} \mathbf{x}_1 \\ \mathbf{x}_2 \end{Bmatrix} + \begin{bmatrix} \mathbf{B}_1 \\ \mathbf{B}_2 \end{bmatrix} \{\mathbf{u}\} \tag{26}$$

where $\mathbf{0}$ is an n-by-n zero matrix.

$$\text{defining}: \dot{\tilde{\mathbf{x}}} = \begin{Bmatrix} \dot{\mathbf{x}}_1 \\ \dot{\mathbf{x}}_2 \end{Bmatrix}, \tilde{\mathbf{A}} = \begin{bmatrix} \mathbf{A} & \mathbf{0} \\ \mathbf{0} & \mathbf{A} \end{bmatrix}, \tilde{\mathbf{x}} = \begin{Bmatrix} \mathbf{x}_1 \\ \mathbf{x}_2 \end{Bmatrix}$$

and the augmented input matrix

$$\tilde{\mathbf{B}} = \begin{Bmatrix} \mathbf{B}_1 \\ \mathbf{B}_2 \end{Bmatrix} \tag{27}$$

The input matrix for the full (ideal) system has the form

$$\mathbf{B}_1 = \begin{Bmatrix} \mathbf{0} \\ \mathbf{M}^{-1}\mathbf{L}_f \end{Bmatrix} \tag{28}$$

$\mathbf{L}_f = \mathbf{M}\phi_n$ is the full left eigenvector for the nth mode

Thus we can rewrite (28):

$$\mathbf{B}_1 = \begin{Bmatrix} \mathbf{0} \\ \phi_n \end{Bmatrix} \tag{29}$$

The input matrix for the truncated system

$$\mathbf{B}_2 = \begin{Bmatrix} \mathbf{0} \\ \mathbf{M}^{-1}\left(\mathbf{L}_{ta} + \Psi\mathbf{p}\right) \end{Bmatrix} \tag{30}$$

$\mathbf{L_{ta}}$ is the truncated left eigenvector for the nth mode using the truncated actuation DOFs. Here, zeroes are inserted to replace DOF where no electrode forcing is applied.

The proposed admissible actuator correction shape has the form

$$\Psi \mathrm{p} = \sum_{i=1}^{k} \Psi_{\mathbf{i}} p_i \tag{31}$$

The matrix of the correction shape functions for the truncated modal actuator is $\Psi = [\Psi_{\mathbf{1}}, \Psi_{\mathbf{2}}, \Psi_{\mathbf{3}}, \ldots, \Psi_{\mathbf{k}}]$ and the vector $\mathbf{P} = \left[p_1, p_2, p_3, \ldots, p_k\right]^T$ contains the weighting factors.

Finally we obtain the augmented state-space equation:

$$\dot{\tilde{x}} = \tilde{\mathbf{A}}\tilde{\mathbf{x}} + \tilde{\mathbf{B}}\left(\mathbf{P}\right)\mathbf{u} \tag{32}$$

The augmented output equation is now:

$$\tilde{\mathbf{y}} = \left[\mathbf{C_f} \; -\mathbf{C_t}\right] \begin{Bmatrix} \mathbf{x_1} \\ \mathbf{x_2} \end{Bmatrix} \triangleq \left\{\mathbf{y_1} - \mathbf{y_2}\right\} \tag{33}$$

Define the output matrix:

$$\tilde{\mathbf{C}} = \left[\mathbf{C_f} \; -\mathbf{C_t}\right] \tag{34}$$

where

$$\mathbf{C_f} = \mathbf{L_f^T}\left[\mathbf{I} \quad \mathbf{0}\right] \tag{35}$$

$$\mathbf{C_t} = \{\mathbf{L_{ts}} + \chi\mathbf{R}\}^T\left[\mathbf{I} \quad \mathbf{0}\right] \tag{36}$$

where: $\mathbf{0}$ and $\mathbf{I}$ are n-by-n zero and identity matrices, respectively.

$\mathbf{L_{ts}}$ is the truncated left eigenvector for the nth mode using the truncated sensing DOFs. Here, zeroes are inserted to replace DOF where no electrode sensing is applied.

The proposed admissible sensor correction shape has the form

$$\chi\mathbf{R} = \sum_{i=1}^{k} \chi_{\mathbf{i}} R_i \tag{37}$$

The matrix of the correction shape functions for the truncated modal sensor is $\chi = [-\Psi_{\mathbf{1}}, -\Psi_{\mathbf{2}}, -\Psi_{\mathbf{3}}, \ldots, -\Psi_{\mathbf{k}}]$ and the vector $\mathbf{R} = [R_1, R_2, R_3, \ldots, R_k]^T$ contains the weighting factors.

Thus the output displacement

$$\tilde{\mathbf{y}} = \tilde{\mathbf{C}}\left(\mathbf{R}\right)\tilde{\mathbf{x}} \tag{38}$$

Using the augmented Lyapunov equation:

$$\tilde{\mathbf{A}}\mathbf{X} + \mathbf{X}\tilde{\mathbf{A}}^{\mathbf{T}} + \tilde{\mathbf{B}}W\tilde{\mathbf{B}}^{\mathbf{T}} = 0 \tag{39}$$

We can find the output response's covariance which is in effect the covariance of the deviation between the truncated and the reference models:

$$J = \tilde{\mathbf{C}}\mathbf{X}\tilde{\mathbf{C}}^{\mathbf{T}} \tag{40}$$

The optimization procedure can be performed while keeping the computational requirements relatively low. The saving in computational effort is enhanced by computing the gradient of the cost function and by solving efficiently with the Lyapunov equation by means of a spectral decomposition, as described in Appendix A.

The unconstrained nonlinear optimization problem is solved by means of a quasi-Newton method which is part of the MatLab™ (2007) optimization toolbox (see fminunc in Matlab users's guide version 2007b).

2.5 The actuator and sensor design criteria

The optimization processes seeks the sensor and actuator electrode correction shapes that minimize J in (40). A shape optimization problem is performed to obtain the optimal weighting factors of all the admissible actuator-Ψ and sensor-χ correction shape functions. Only five correction shape functions of constant and slope are chosen in this work, the practical meaning of the selected shaping functions is to be able to realize a simple mechanism for trimming that affect only the lower modes.

3 A one dimensional example—bending of a beam

Figure 1 shows an illustration of a clamped-clamped beam with truncated modal electrodes:

The beam vibrations are excited and sensed by distributed spatial electrodes along the beam acting on both sides. The spacing of the electrodes from the beam is the design variable $d_0(x)$. Other design variables are the number of electrode segments needed for actuation and sensing of a specific mode.

The actuator and sensor are designed to be sensitive only to the third vibration mode, and to filter out signals from all other modes. For sake of simplicity, we limit our discussion to the extraction of the third mode shape function of the beam. Of course, the method described here can be applied to other mode shapes as well to combinations of modes.

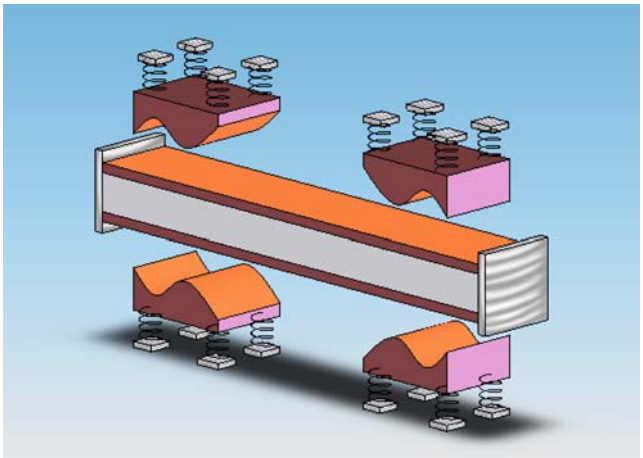

Fig. 1 Illustration of the segmented shaped modal electrodes

The chosen beam length is $L = 10$ [μm] and it is divided into $N = 100$ elements. The mechanical properties of the beam are: $E = 150 \times 10^3 \left[\mu\text{Newton}/\mu\text{m}^2\right]$, area cross section $A = b \times h = 0.1 \times 0.1 \left[\mu m^2\right]$, moment of inertia $I = \frac{bh^3}{12} \left[m^4\right]$ and the density $\rho = 2{,}330 \times 10^{-18} \left[\text{kg}/\mu\text{m}^3\right]$.

The computed third left eigenvector $\mathbf{l}_3 = \mathbf{M}\phi_3$ gives the distribution of a spatial external force needed to excite only the third mode of the beam. Using the shape functions (third-order Hermitian polynomials defined in Geradin and Rixen 1998), the spatial force distribution can be computed. This force distribution is depicted in Fig. 2.

As evident in Fig. 2, the force changes its sign along the beam, but the electrostatic force can only cause attractive forces. It can thus be concluded from Fig. 2 that the electrodes must be divided into three separate regions. Zero force level translates into a high electrode gap thus one can create a gap between the electrodes at these locations. After calculating the external force we can derive the electrode gap. It is now possible to design the configuration and location of the actuation and sensing electrodes according to the required spatial force distribution. This segmentation is illustrated in Fig. 3.

A logical approach is to get as much spatial information as possible from the structure. It is for this purpose that one should design the segments of electrodes to cover a maximal area on the structures. But, in our example the chosen optimization problem was made more difficult by configuring the segments of the actuators/sensors electrodes to be smaller then the feasible ones. The electrodes were designed to cover the regions of: $0.5 \le x \le 2$, $4 \le x \le 6$, $8 \le x \le 9.5$ as shown in Fig. 3. Indeed, the actual implementation of the electrodes does not act on all the available DOF and is therefore truncated. It is clear that the resulting force and the response are somewhat different than the ideal distribution.

3.1 Simulation of the beam frequency response before and after electrode optimization

The simulation of the double clamped (C–C) beam using a truncated modal actuator/sensor and an ideal full modal electrode is described here. The electrode design attempts to isolate the third mode shape, a task that is not performed well by the truncated electrode. The frequency response is shown in Fig. 4:

It is clear that truncation has resulted in the excitations of undesired modes. The use of a combination

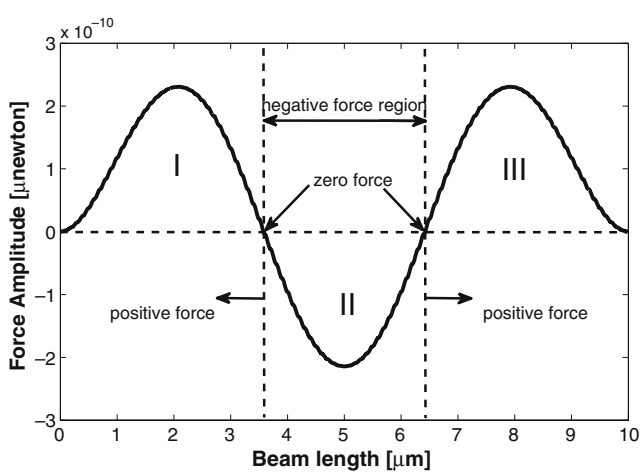

Fig. 2 Left eigenvector—distribution of a spatial external force

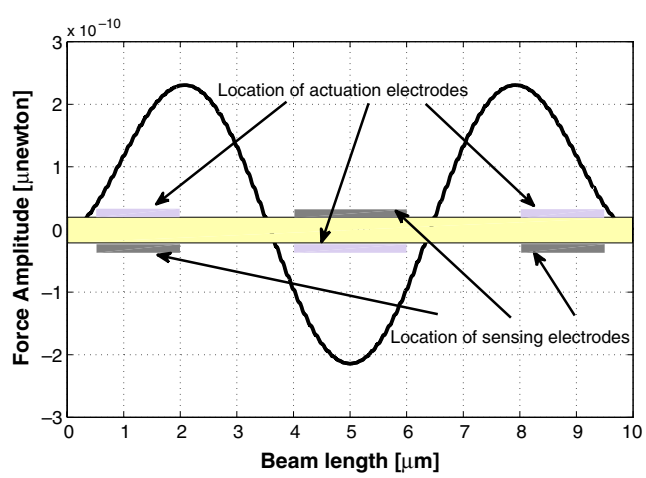

Fig. 3 Locations of the actuator/sensor electrodes

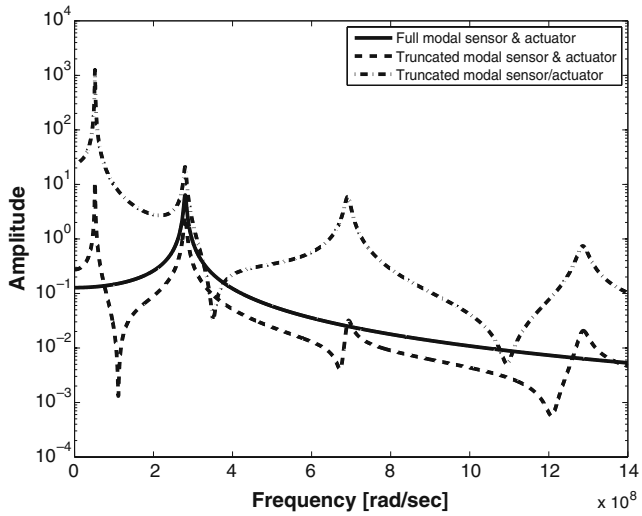

Fig. 4 FRF—truncated modal electrodes (before optimization)

of a modal actuator and a modal sensor is preferred because it doubles the spatial filter effect. It is seen from Fig. 4, that a combination of truncated modal actuator and modal sensor has higher selectivity of modes than just using one of them.

The optimization or trimming of the truncated electrode is affects the FRF that becomes closer to the ideal one. The resulting FRF after optimization is shown in Fig. 5.

As can be observed from Fig. 5 the optimized FRF is very close to the ideal FRF. Figure 5 shows that truncated modal filter results in imperfect filtering, while the optimized result that was obtained after trimming the shape of the actuator and sensor electrodes seems considerably better. The weighting (trimming) values of the parameters (P) and (R) from the optimization process are summarized in Table 1:

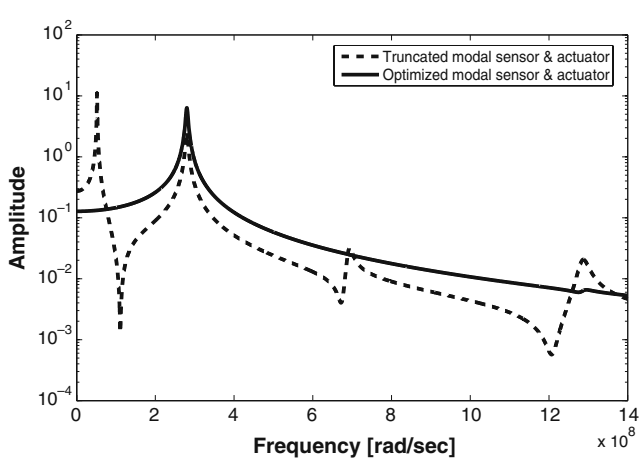

Fig. 5 FRF—after optimization

According to Table 1 five shape functions were defined, the selected correction shaping functions for the truncated model is:

$\{\Psi_1\}$ Constant vector defined on the center actuator electrode DOF
$\{\Psi_2\}$ Constant vector defined on the two sides actuator electrodes DOF
$\{\Psi_3\}$ Symmetric slope vector defined on the sides actuator electrodes DOF
$\{\Psi_4\}$ Positive slope vector defined on the center actuator electrode DOF
$\{\Psi_5\}$ Negative slope vector defined on the center actuator electrode DOF

The practical meaning of the selected simple shaping functions of constant and slope is to be able to realize a mechanism for trimming. The slope vectors correction Ψ_3, Ψ_4, Ψ_5 improve the system response function and facilitated to decrease the high frequency undesired modes.

The trimmed electrodes of the actuator electrode are described graphically, in Fig. 6 and it was derived from (17).

4 Optimal design of a RF MEMS filter by a free–free micromechanical 3D-structure

This chapter describes the proposed design and the simulation of a 3D spatial modal sensor and actuator on a 3D-mechanical filter, which is illustrated in Fig. 7. A three-dimensional finite element model was formed to inspect a certain vibrational mode pattern and to provide accurate predictions to possible spurious oscillation mode. A spurious mode (using the terminology from Nguyen et al. (2000)) arises when the torsional suspension exhibit an additional flexural motion causing the support area to vibrate like a trampoline. This mode is being excited and sensed due to the truncation of the exciting electrodes.

A high quality factor-Q (low damping) is desired in many applications as this improved the signal to noise ratio. In order to maximize the Q of a given resonator design, the energy lost coupling through the supports must be minimized. For this purpose, quarter wavelength torsional suspensions are often used to mount the structure at the nodal points (Nguyen et al. 2000). It will be shown below that the concept of quarter wavelength must be modified when dealing with 3D structures.

The typical dimensions of the proposed model are: Lr = 14.3 [μm] length, Wr = 6 [μm] width, T = 4.2 [μm] thickness, $A_s = 1 \times 1$ [μm^2] cross section of the support beam.

Table 1 Weighting values of the parameters (P) and (R)

P_1	P_2	P_3	P_4	P_5	R_1	R_2	R_3	R_4	R_5
−0.0015	−0.0087	0.0384	0.0652	0.0652	0.0639	−0.0289	0.0144	0.0782	0.0782

The model mechanical properties of polysilicon are:

$$E = 150 \times 10^3 \left[{}^{\mu\text{Newton}}/_{\mu\text{m}^2} \right],$$

$$\upsilon = 0.226, \rho = 2,330 \times 10^{-18} \left[{}^{\text{kg}}/_{\mu\text{m}^3} \right]$$

The operational vibration mode of the filter is mode number 15 at frequency of $f = 1.36 \times 10^8$ [Hz].

4.1 Support structure design method

The best supporting structure will not burden it at the operating frequency thus giving rise an effective free–free structure. The purpose of this analysis is to determine the nodal points, mode shapes and natural frequencies for the beam. Nodal points provide a support location where no lateral motion takes place and thus no mechanical work is being performed on the support thus energy losses are minimized.

The first three mode shapes for a free–free beam with the corresponding node locations are shown in Fig. 8.

The mode shapes in Fig. 8 have been arbitrarily normalized to have a maximum value of unity. The supported beams are mounted to the body which is basically a free–free beam vibrating in the fundamental flexural mode.

In reality, the support always causes some leakage of mechanical energy. In order to minimize these energy losses, the support lengths must be carefully optimised.

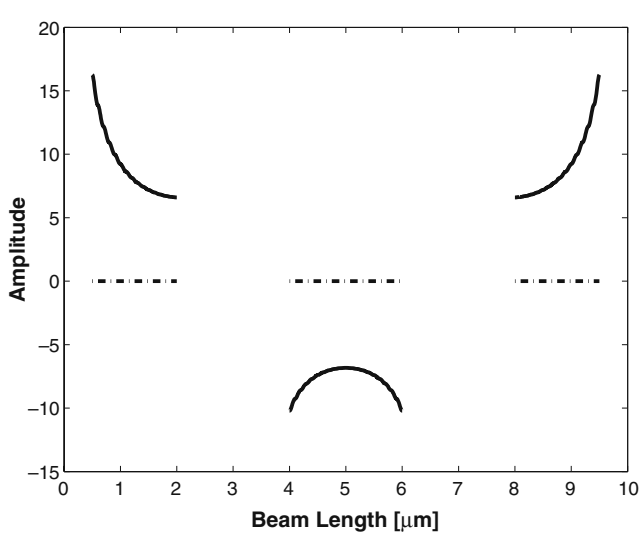

Fig. 6 Actuator electrode gap

Ideally the suspension beams should experience only torsional motion in the mode of operation, meaning that the lengths of the support beams are chosen to correspond to the effective 'quarter-wavelength' of the support local resonance frequency. In addition, the analytical solution of the quarter wave length approach was compared to a numerical parametric design method. The following result shows that for a 3D model the analytical solution has no meaning and it therefore explains the inferior performance that was reported by previous researchers.

4.1.1 Analytical investigation of the quarter wave length approach

Consider a clamped-free round shaft in torsion, the solution yields the ratio between the length of the shaft and the wavelength at resonance:

$$L = \left(\frac{1}{4} + \frac{n}{2} \right) \lambda \tag{41}$$

Choosing the first (fundamental) mode, $n = 0$ in (41) , gives the quarter wavelength

$$L = \frac{1}{4} \lambda \tag{42}$$

Using (42) we can find the length of the circular shaft corresponding to a quarter wavelength

$$L = \frac{1}{4f} \sqrt{\frac{G}{\rho}} \tag{43}$$

A shaft of rectangular cross section, due to the warping of the cross section during twist, a change to the

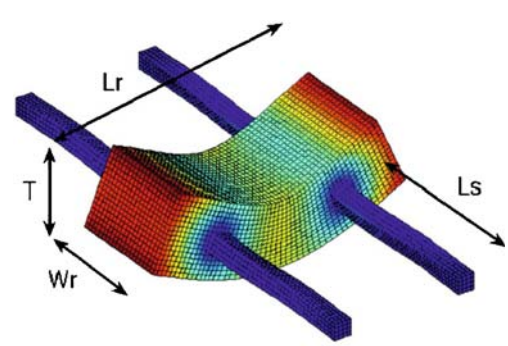

Fig. 7 3D filter model operating mode

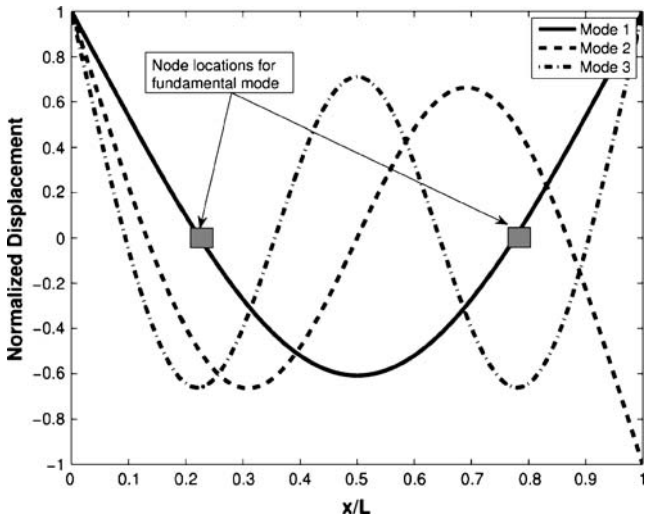

Fig. 8 Modes of free–free beam

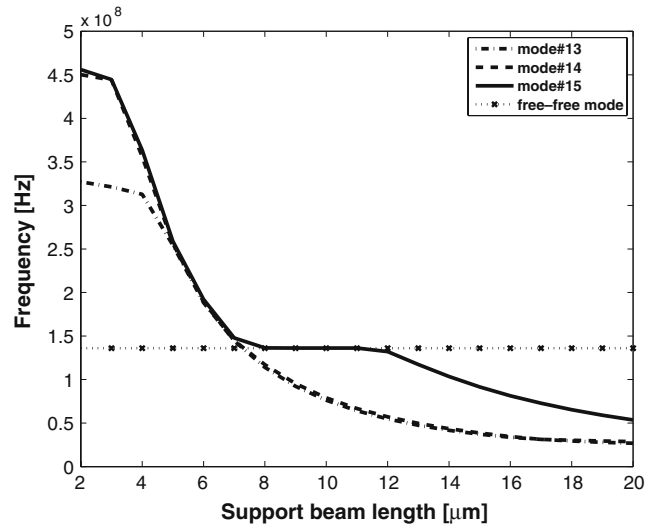

Fig. 9 Support beam length

torsional rigidity of the circular shaft has to be calculated from Timoshenko (1958). Knowing the support beam's width $S_w = 1$ [μm] and support beam's height $S_h = 1$ [μm], the ratio $\frac{S_h}{S_w} = 1$ therefore the numerical factor $\beta = 0.141$ and the torsion correction constant $\gamma = \beta S_h S_w^3 = 0.141$. Thus the length of a shaft with rectangular cross section is

$$L = \frac{1}{4f}\sqrt{\frac{G\gamma}{\rho}} \tag{44}$$

Where, the shear modulus of elasticity $G = \frac{E}{2(1+\upsilon)}$. The calculated optimal length of the shaft for the applied properties of the support beam is $L = 3.5$ [μm].

4.1.2 Optimisation of the support structure length using a numerical parametric design method

The numerical optimisation modifies the actual parameter length of the supports (Ls) until the obtained natural frequency for the operating mode is as close as possible to the free–free structure. It is assumed that the best support would not perform any work on the structure and therefore will not alter the natural frequency. The theoretical quarter length design was used as the initial value. The structural part consists of finite-element model with a 3D isotropic-material elements imported from Ansys™ into Matlab™ by using SDT (Balmes 2007), the simulation was carried

Fig. 10 Spatial external force 3D-distribution

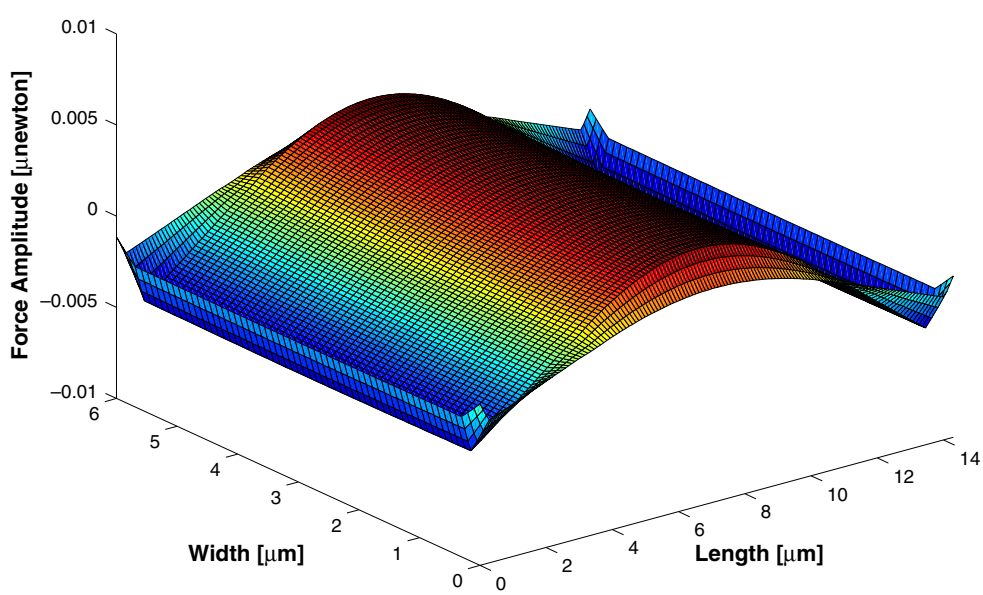

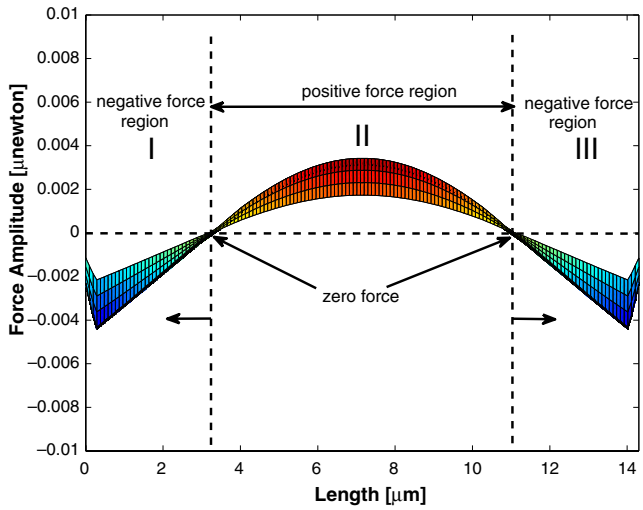

Fig. 11 Section view—spatial external force distribution

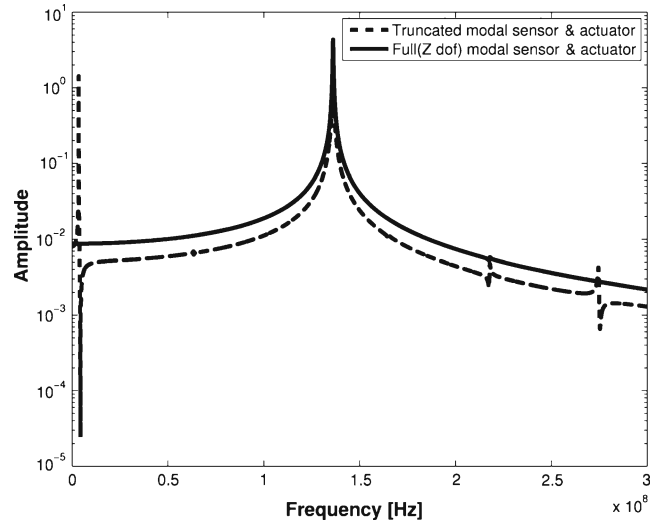

Fig. 13 3D-model FRF—truncated modal electrodes

out in Matlab^{TM}. The geometry is described in Fig. 7. The nodal points were calculated analytically where we attached four support beams to the body. The result of a parametric investigation is shown in Fig. 9.

Figure 9 presents simulated plots, using variations of the support beam length dimension, of frequency versus support beam length. The horizontal line describes the free–free beam operating in the relevant mode. The intersection of mode number 15 and the horizontal line gives the desired length of the support beam, Ls = 11 [μm]. This length of the support beams is effectively a quarter wave lengths thus the body behaves like a free–free beam. The theoretical quarter wavelength design did not produce a free–free structure as evident from (Fig. 10). This can be explained by the fact that the true dynamical behaviour is three-dimensional and the assumption that only torsion takes place is erroneous.

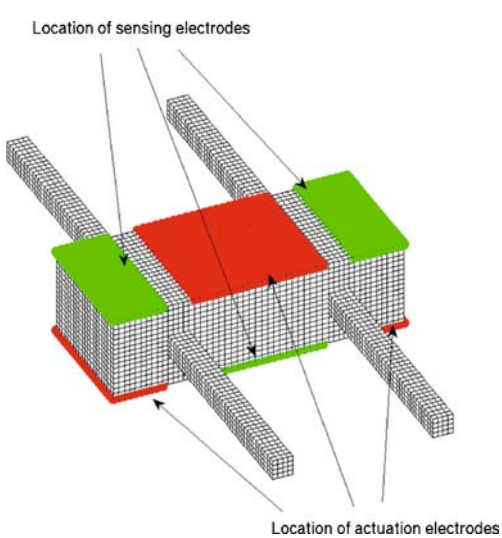

Fig. 12 Locations of the actuator/sensor electrodes

4.2 Spatial force distribution and configuration of the actuation/sensing electrodes

The actuator and sensor are designed to be sensitive only to the operational mode of vibration-mode number 15, and filter out signals from all other modes. In order to excite the n'th-mode while the remaining modes are not excited, one needs to define the distributed force on the RHS from the equation of motion as explained before. This force is proportional to the computed left eigenvector $\boldsymbol{l}_{15} = \mathbf{M}\boldsymbol{\phi}_{15}$ that gives the 3D-distribution of a spatial external force needed to excite only this mode. Using interpolation based on the element shape functions and a fine grid resolution, the faithful reconstruction of the spatial force can be computed as is shown in Fig. 10.

From the force 3D-distribution and due to the symmetry of the model we can look at a section view that

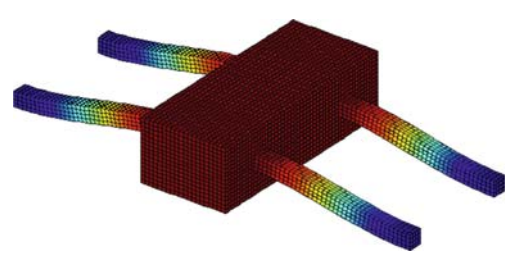

Fig. 14 Fundamental vibration mode

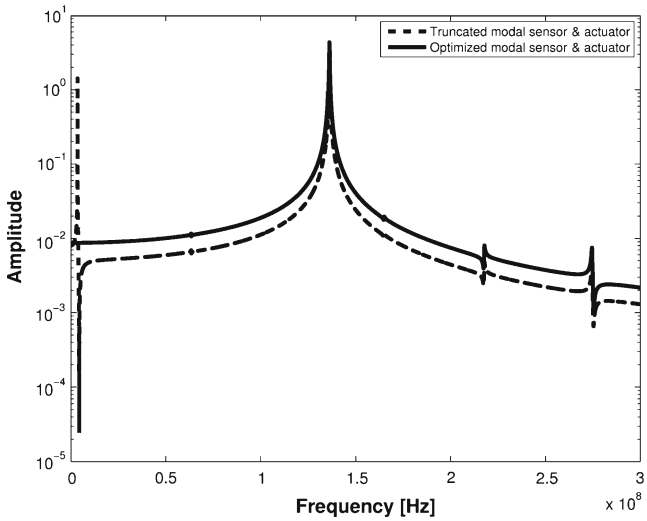

Fig. 15 3D-model FRF after optimization

represents the force distribution along the length and is shown in Fig. 11.

Clearly, as shown in Fig. 11, the force changes its sign along the length, but the electrostatic force can only attract. It can thus be concluded from Fig. 11 that the electrodes must be divided into 3 separate regions. We can now design the configuration of the actuation and sensing electrodes that implement the desired spatial force distribution. This is illustrated in Fig. 12.

On the basis of the expression for the electrostatic force's spatial distribution that acts on the elements nodes to excite only the desired mode ϕ_n, the geometry of the electrode can be derived directly from (16):

$$d_0\,(x,\,y) = \sqrt{\left|\frac{\mathrm{V_{con}}}{f_{\mathbf{e}}}\right|} \tag{45}$$

Using (45) the electrode gap parameter can now be computed.

4.3 Simulation of the 3D-model frequency response before and after electrode optimization

The ideal full modal-electrode consists of the entire model DOFs,. i.e. 3 DOF per node, in this case. The electrode, on the other hand, acts only in z direction and therefore the truncated modal electrodes produce the frequency response which is different than the desired one, as shown in Fig. 13.

It is clear that the truncation of the modal electrode has resulted in the excitations of an undesired mode at a low frequency as shown in Fig. 14:

Indeed, it has been observed that contamination due to unmodeled dynamics (the mismodelling often stems from using lumped electrical model to describe 3D structures) can lead to spurious vibrational modes described in Nguyen et al. (2000). This incomplete model can degenerate the performance, if coupled to the desired high-Q mode of the filter. The proposed trimming approach reduces this problem and the simulation of the 3D-model for the optimized actuator/sensor

Fig. 16 Actuator electrode gap

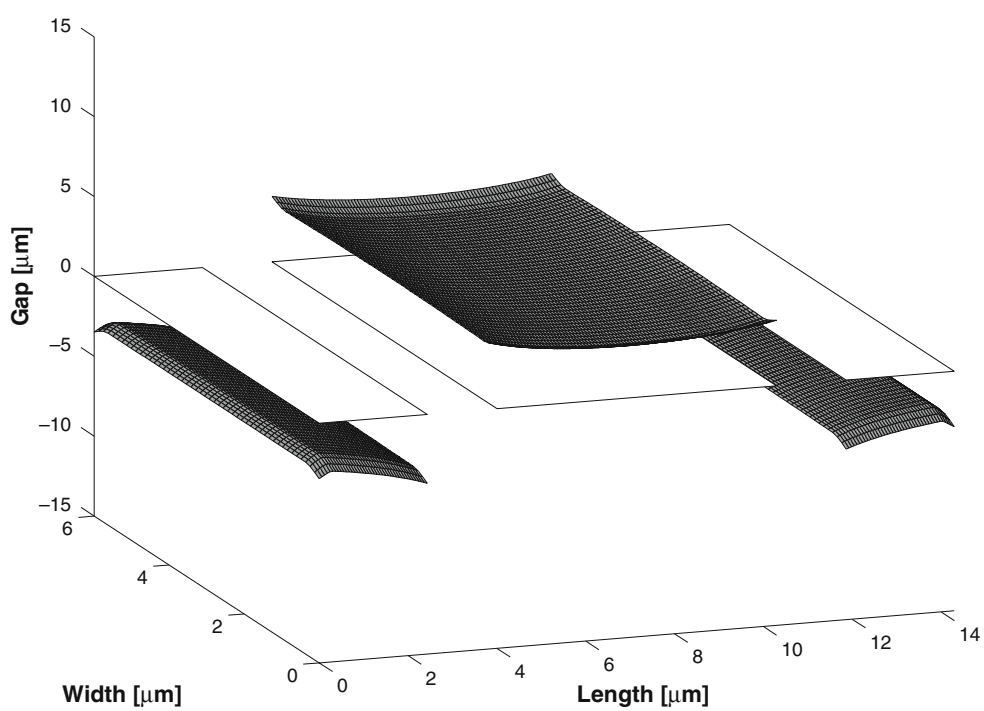

electrodes was performed. The resulting FRF after optimization is shown in Fig. 15.

As can be observed from Fig. 15, the obtained, optimized FRF is very close to the ideal FRF. The results were obtained after trimming the shape of the actuator and sensor electrodes.

The actuator electrode gap that excites the operational mode is shown in Fig. 16 as was derived from (45).

Figure 16 show the gap geometry of the actuator electrodes that excites the specific mode.

The sensor electrode gap for sensing the operational mode is shown in Fig. 17 as was derived from (45).

Figure 17 shows the gap geometry of the sensor electrodes that detect the specific mode.

5 The effect of optimization on cancellation of unwanted poles with zeros

The trimming process affects the system's dynamics in a particular manner by affecting the zeroes. The poles and zeros of a system are defined in terms of the transfer function:

$$H(s) = \frac{\prod_{i=1}^{Nz}(s+z_i)}{\prod_{j=1}^{Np}(s+p_j)} \tag{46}$$

The first five poles and zeros locations for the truncated and the optimized systems are summarized in Table 2.

The calculation of the poles (natural frequencies) and zeros (anti-resonance) is carried out by seeking the roots of the relevant polynomials in the truncated and optimized systems.

The optimization of the shaped spatial force has influenced the zero location of the optimized system, the poles are the system characteristic frequencies and they are not changed. Thus the idea of cancellation of poles with zeros is realized. Table 2 shows for i.e. the cancellation of the pole at 3.474 [MHz] by a zero. Controlling the poles and zeros gives the ability to design a system with desired properties and frequency response. However, when a transfer function of a physical system is considered, it is very unlikely that the pole and zero would remain in exactly the same place, a minor tolerance change in the electrodes or structure, for instance, could cause one of them to move just slightly. If this occurs, a simple trimming mechanism for the electrodes with linear and angular motion can rectify this problem, exactly like in the optimization procedure. The calibrated error correction mechanism can be realized with a comb-drive with suspensions for the static electrode thus applying external voltage would create linear and angular trimming as needed. Near cancellation of pole and zero may indeed render the system sensitive to external disturbances

Fig. 17 Sensor electrode gap

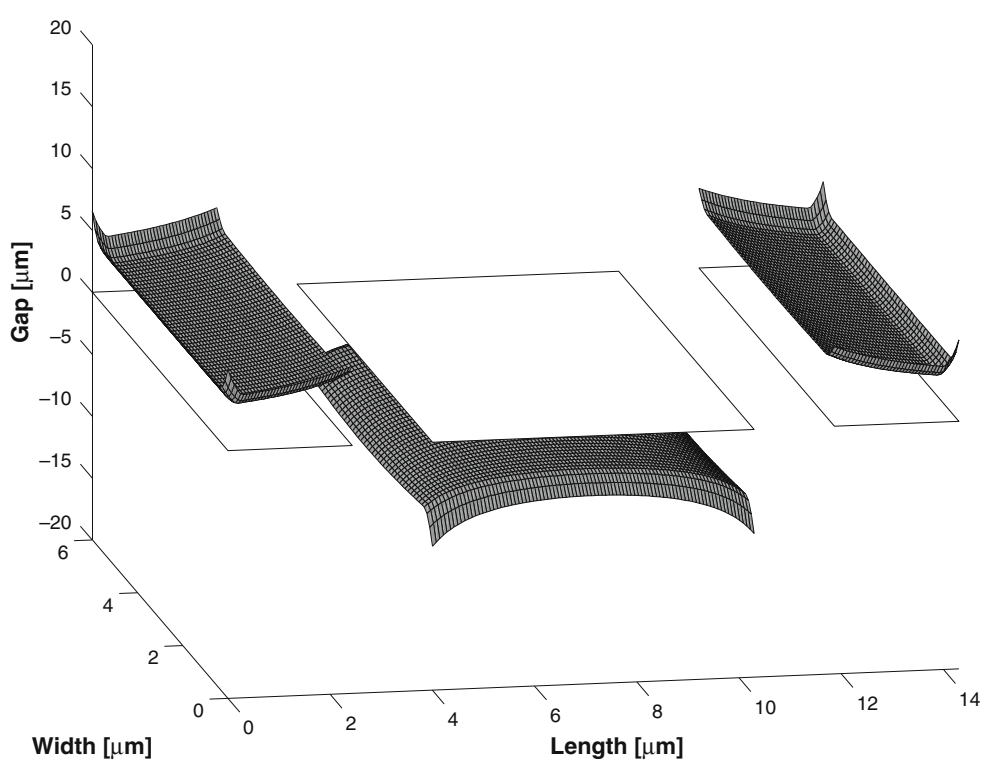

Table 2 Pole-zero location for 3D model example

Truncated system		Optimized system	
Poles (MHz)	Zeros (MHz)	Poles (MHz)	Zeros (MHz)
3.472	3.474	3.472	3.472
3.474	3.915	3.474	3.474
3.915	4.328	3.915	3.915
13.748	13.748	13.748	13.748
34.050	34.050	34.050	34.050

under feedback control, in extreme cases it can even become unstable. In the present case, the system operates in open loop thus this extreme condition is of a much lesser importance as it can be eliminated by trimming.

6 Conclusions

This paper shows the importance of precise, 3D modelling for the accurate design of electromechanical (MEMS) filters. A numerically efficient trimming procedure was developed to design segmented spatial sensors/actuators electrodes that quickly performs modal filtering. The function of trimming was explained by inspection of the zero locations and it was shown that spurious modes are eliminated by this process via pole-zero cancellation.

The role of accurate modelling was further emphasized when a quarter wavelength type of support was designed. It was shown numerically that the analytical one-dimensional model that is used for torsion-beam supports, can provide inferior designs. Still, a numerical optimization, making use of full 3D modelling, has resulted in a supporting structure that performs effectively like a quarter wave length support.

Throughout this paper, we provided a physical insight to the various aspects related to the modal transducers. The procedure is relatively simple and can be performed to keep computation requirements relatively low.

Uncertainties due to variable temperature during time of operation and drift in the boundary conditions can be added as robustness parameters in the optimization process.

Appendix

Solving an augmented Lyapunov equation by spectral decomposition

This appendix described the efficient solution method of the Lyapunov equation that needs to be solved during the optimization. The equation has the form:

$$\mathbf{AX} + \mathbf{XG} + \mathbf{Q} = 0 \tag{47}$$

where:

$$\mathbf{A} = \begin{bmatrix} \mathbf{0} & \mathbf{I} \\ -\mathbf{M}^{-1}\mathbf{K} & -\mathbf{M}^{-1}\mathbf{D} \end{bmatrix}$$

In large dynamical models, it is often the case that a few modes are computed so this spectral decomposition (as introduced in Bucher and Braun 1993) simplifies the solution strategy.

But, here we need to solve an augmented Lyapunov equation that has a special spectral decomposition. The augmented Lyapunov equation is:

$$\widetilde{\mathbf{A}}\widetilde{\mathbf{X}} + \widetilde{\mathbf{X}}\widetilde{\mathbf{A}}^{\mathbf{T}} + \widetilde{\mathbf{B}}W\widetilde{\mathbf{B}}^{\mathbf{T}} = 0 \tag{48}$$

Where:

$$\widetilde{\mathbf{A}} = \begin{bmatrix} \mathbf{A} & \mathbf{0} \\ \mathbf{0} & \mathbf{A} \end{bmatrix}, \ \widetilde{\mathbf{B}} = \begin{Bmatrix} \mathbf{B_1} \\ \mathbf{B_2} \end{Bmatrix}$$

$$\begin{aligned} &\widetilde{\mathbf{Q}} = \left\{\widetilde{\mathbf{B}}\right\}\left\{\widetilde{\mathbf{B}}\right\}^T \ \left\{\widetilde{\mathbf{B}}\right\} \in \mathbb{R}^{4n} \\ &n = \text{no. of DOF in FE model} \end{aligned} \tag{49}$$

The spectral decomposition of matrix $\widetilde{\mathbf{A}}$ can be formulated using the eigenvalues and eigenvectors, thus we can compute the modal matrix of $\widetilde{\mathbf{A}}$ that has the form:

$$\widetilde{\mathbf{U}}_{\mathbf{A}} = \begin{bmatrix} \phi & \phi & 0 & 0 \\ \phi\Lambda_1 & \phi\Lambda_2 & 0 & 0 \\ 0 & 0 & \phi & \phi \\ 0 & 0 & \phi\Lambda_1 & \phi\Lambda_2 \end{bmatrix} \tag{50}$$

The eigenvalues of matrix $\mathbf{A}$ are

$$\begin{aligned} \Lambda_1 &= diag\left\{-\zeta_r\omega_r\right\} + jdiag\left\{\sqrt{1-\zeta_r^2}\omega_r\right\} \\ \Lambda_2 &= diag\left\{-\zeta_r\omega_r\right\} - jdiag\left\{\sqrt{1-\zeta_r^2}\omega_r\right\} \end{aligned} \tag{51}$$

Thus the inverse of the modal matrix $\widetilde{\mathbf{U}}_{\mathbf{A}}^{-1}$

$$\widetilde{\mathbf{U}}_{\mathbf{A}}^{-1} = \begin{bmatrix} (\Lambda_2-\Lambda_1)^{-1}\Lambda_2\phi^{-1} & -(\Lambda_2-\Lambda_1)^{-1}\phi^{-1} & 0 & 0 \\ -(\Lambda_2-\Lambda_1)^{-1}\Lambda_1\phi^{-1} & (\Lambda_2-\Lambda_1)^{-1}\phi^{-1} & 0 & 0 \\ 0 & 0 & (\Lambda_2-\Lambda_1)^{-1}\Lambda_2\phi^{-1} & -(\Lambda_2-\Lambda_1)^{-1}\phi^{-1} \\ 0 & 0 & -(\Lambda_2-\Lambda_1)^{-1}\Lambda_1\phi^{-1} & (\Lambda_2-\Lambda_1)^{-1}\phi^{-1} \end{bmatrix} \tag{52}$$

Using the definition $\phi^{-1} = \phi^T M \triangleq L^T$,we prevent the explicit numerical inversion of the modes. Instead we make use of the left eigenvectors.

Defining

$$\widetilde{\mathbf{Y}} = \widetilde{\mathbf{U}}_{\mathbf{A}}^{-1}\widetilde{\mathbf{X}}\widetilde{\mathbf{U}}_{\mathbf{G}} \tag{53}$$

Where $\widetilde{\mathbf{U}}_{\mathbf{G}}$ is the modal matrix of $\widetilde{\mathbf{A}}^{\mathbf{T}}$, we can derive the expression for every entry

$$\widetilde{Y}_{i,j} = \frac{-\left[\widetilde{\mathbf{U}}_{\mathbf{A}}^{-1}\widetilde{\mathbf{Q}}\widetilde{\mathbf{U}}_{\mathbf{G}}\right]_{i.j}}{\lambda_{\widetilde{A}i} + \lambda_{\widetilde{G}i}} \tag{54}$$

The computation of the solution for the Lyapunov equation is thus straightforward:

$$\widetilde{X} = \widetilde{\mathbf{U}}_{\mathbf{A}}\widetilde{Y}\widetilde{\mathbf{U}}_{\mathbf{A}}^{\mathbf{T}} \tag{55}$$

By defining:

$$\widetilde{\mathbf{P}} = \widetilde{\mathbf{U}}_{\mathbf{A}}^{-1}\{\widetilde{\mathbf{B}}\} \quad \text{where} \quad \widetilde{\mathbf{U}}_{\mathbf{G}} = \left(\widetilde{\mathbf{U}}_{\mathbf{A}}^{-1}\right)^T \tag{56}$$

The memory storage requirements are reduced to practical levels. Using (56), we can evaluate in a straightforward manner

$$\widetilde{Y}_{i,j} = \frac{-\left[\widetilde{\mathbf{P}}\widetilde{\mathbf{P}}^{\mathbf{T}}\right]_{i.j}}{\lambda_{\widetilde{A}i} + \lambda_{\widetilde{G}i}} \tag{57}$$

And we can find the output response covariance:

$$J = \widetilde{\mathbf{C}}\widetilde{\mathbf{X}}\widetilde{\mathbf{C}}^{\mathbf{T}} \tag{58}$$

And finally the cost function can be evaluated from:

$$J = \left(\widetilde{\mathbf{C}}\widetilde{\mathbf{U}}_{\mathbf{A}}\right)\widetilde{Y}_{i,j}\left(\widetilde{\mathbf{C}}\widetilde{\mathbf{U}}_{\mathbf{A}}\right)^T \tag{59}$$

References

Balmes E (2007) Structural dynamics toolbox for Matlab, User's guide ver.6, http://www.sdtools.com

Bao MH (2000) Handbook of sensors and actuators. Micro mechanical transducers: pressure sensors, accelerometers and gyroscopes, vol 8. Elsevier

Bucher I, Braun S (1993) The structural modification inverse problem: an exact solution. Mech Syst Signal Process 7(3):217–238

Bucher I, Braun S (1997) Left-eigenvectors: extraction from measurements and physical interpretation. ASME transactions. J Appl Mech 64:97–105

Callahan J, Baruh H (1996) Active control of flexible structures by use of segmented piezoelectric elements. J Guid Control Dyn 19(4):808–815

Callahan J, Baruh H (1999) Modal sensing of circular cylindrical shells using segmented piezoelectric elements. Smart Mater Struct 8:125–135

Friswell MI (1999) Partial and segmented modal sensors for beam structures. J Vib Control 5:619–637

Friswell MI (2001) On the design of modal actuators and sensors. J Sound Vib 241(3):361–372

Gawronski W (1998) Dynamics and control of structures, A modal approach. Springer, New York

Gawronski W (2000) Modal actuators and sensors. J Sound Vib 229(4):1013–1022

Geradin M, Rixen D (1998) Mechanical vibrations—theory and application to structural dynamics, 2nd edn. Wiley

He J, Fu Z-F (2001) Modal analysis. Butterworth Heinemann

John D, Jerman H, Thomas W (2003) Design of large deflection electrostatic actuators. IEEE ASME J Microelectromech Syst 12(3):335–343

Kim J, Ryou J (2002) Optimal gain distribution for two-dimensional modal transducer and its implementation using multi-layered PVDF films. J Sound Vib 251(3):395–408

Kim SJ, Hwang JS, Mok J (2000) Sensor/actuator optimal design for active vibration control of shell structure. J Intell Mater Syst Struct 11

Mao Q (2004) Theoretical development and experimental validation of modal sensors. Acoust Sci Tech 25(1):81–84

Matlab (2007) Optimization toolbox for Matlab, User's guide ver.2007b

Michael L, Mauro J (2001) Review of modal sensing and actuation techniques. Shock Vibr Dig 33(1):3–14

Nguyen C, Wang K, Wong A-C (2000) VHF free–free beam high-Q micromechanical resonators. J Micromech Syst 9(3): 347–360

Preumont A (1997) Vibration control of active structures: an introduction. Kluwer Academic, Boston

Preumont A, Francois A, De Man P, Piefort V (2003) Spatial filters in structural control. J Sound Vib 265:61–79

Skelton R (1988) Dynamic systems control: linear system analysis and synthesis. Wiley, New York

Strang G (2006) Linear algebra and its applications, 4th edn. Brooks/Cole

Takagi K, Nagase K, Oshima K, Hayakawa Y (2001) Modal filtering for simply supported plate using equally segmented piezoelectric film. In: Proceedings of the American Control Conference Arlington

Tilmans H (1996) Equivalent circuit representation of electromechanical transducers, part I: lumped parameter system. J Micromech Microeng 6(2):157–176. doi:10.1088/0960-1317/6/1/036

Timoshenko S (1958) Strength of materials, part I: elementary theory and problems, 3rd edn. Melbourne

Zhang Q, Allemang RJ, Brown DL (1990) Modal filter: concept and applications. In: International Modal Analysis Conference, IMAC conference proceedings

Zhuang Y, Baras JS (1994) Shape optimization of distributed sensors and actuators for smart structure control. In: SPIE proceedings, Smart Structures and Materials